



Control of the exciton valley dynamics in atomically thin semiconductors by tailoring the environment

A. Prazdnichnykh, M. Glazov, L. Ren, C. Robert, B. Urbaszek, X. Marie

► To cite this version:

A. Prazdnichnykh, M. Glazov, L. Ren, C. Robert, B. Urbaszek, et al.. Control of the exciton valley dynamics in atomically thin semiconductors by tailoring the environment. Physical Review B, 2021, 103 (8), 10.1103/PhysRevB.103.085302 . hal-03451936

HAL Id: hal-03451936

<https://hal.science/hal-03451936>

Submitted on 26 Nov 2021

HAL is a multi-disciplinary open access archive for the deposit and dissemination of scientific research documents, whether they are published or not. The documents may come from teaching and research institutions in France or abroad, or from public or private research centers.

L'archive ouverte pluridisciplinaire **HAL**, est destinée au dépôt et à la diffusion de documents scientifiques de niveau recherche, publiés ou non, émanant des établissements d'enseignement et de recherche français ou étrangers, des laboratoires publics ou privés.

Control of the exciton valley dynamics in van der Waals heterostructures

A. I. Prazdnichnykh,^{1,2} M. M. Glazov,¹ L. Ren,³ C. Robert,³ B. Urbaszek,³ and X. Marie³

¹*Ioffe Institute, 26 Polytechnicheskaya, 194021 St. Petersburg, Russia*

²*National Research University Higher School of Economics, Saint Petersburg, Russia,*

³*Université de Toulouse, INSA-CNRS-UPS, LPCNO, 135 Avenue Rangueil, 31077 Toulouse, France*

(Dated: October 6, 2020)

The exciton valley dynamics in van der Waals heterostructures with transition metal dichalcogenides monolayers is driven by the long-range exchange interaction between the electron and the hole in the exciton. It couples the states active in the opposite circular polarizations resulting in the longitudinal-transverse splitting of excitons propagating in the monolayer plane. Here we study theoretically the effect of the dielectric environment on the long-range exchange interaction and demonstrate how the encapsulation in the hexagonal boron nitride modifies the exciton longitudinal-transverse splitting. We calculate the exciton spin/valley polarization relaxation due to the long-range exchange interaction and demonstrate that the variation of the monolayer environment results in significant, up to five-fold, enhancement of the exciton valley polarization lifetime.

I. INTRODUCTION

Two-dimensional (2D) materials combined into van der Waals heterostructures offer a versatile platform with unusual optical and transport properties [1, 2]. In the family of the monolayer semiconductors based on transition metal dichalcogenides the optical properties are controlled by robust excitons, Coulomb bound electron-hole pairs [3–11]. Tailoring the environment of the monolayer, e.g., by encapsulation into hexagonal boron nitride (hBN), affects excitonic states [12, 13], optical spectra of atomically-thin semiconductors [14], and makes it possible to control radiative lifetime of excitons [15–18]. It opens wide prospects for nanophotonic applications [19–23].

The direct optical transitions in transition-metal dichalcogenide monolayers involve the electronic states at the edges of the Brillouin zone. The symmetry and spin-orbit interaction enable the so-called chiral selection rules: The band-edge optical transitions at the \mathbf{K}_+ (\mathbf{K}_-) valley are induced by the photon of the σ^+ (σ^-) circular polarization, since valley and spin are locked [24–30]. Accordingly, the optically active excitons possess a valley or pseudospin degree of freedom [7, 9, 31].

The valley dynamics of excitons in transition metal dichalcogenides monolayers is in focus of the experimental and theoretical research nowadays [32–36]. It has been established [31, 38–40] that similarly to the case of conventional quasi-two-dimensional semiconductors where the pseudospin is associated with the spins of electron and hole forming an exciton [41–43], the bright exciton valley dynamics is controlled by the long-range exchange interaction between the electron and the hole. The process of valley depolarization of the exciton can be considered as a virtual recombination of the electron-hole pair in one valley and its emergence in the opposite valley [38, 39].

Since the radiative properties of the excitons can be manipulated in van der Waals heterostructures [15–17], it is natural to ask the question whether the dielectric en-

vironment affects the valley dynamics of excitons in two-dimensional semiconductors. Here we address this question theoretically. We demonstrate that the presence of surrounding hBN layers screens the long-range exchange interaction and slows-down valley depolarization of excitons. We develop a microscopic theory of the effect based on the electrodynamical approach for calculating the exchange interaction in the exciton. We use the density matrix method to study the valley polarization dynamics in transition metal dichalcogenide monolayers. We demonstrate significant, up to a five-fold, increase of the valley polarization lifetime in van der Waals heterostructures depending on the hBN layer thickness. To the best of our knowledge, this control of the exciton spin dynamics by the environment was never demonstrated before in semiconductors.

The paper is organized as follows: Section II presents the calculations of the exciton fine structure due to the long-range exchange interaction in van der Waals heterostructures. Next, in Sec. III the valley dynamics of the excitons is calculated and analyzed. Various regimes of valley polarization decoherence depending on the systems' parameters are identified and analyzed. The concluding remarks are presented in Sec. IV.

II. EXCITON FINE STRUCTURE

This section presents the microscopic theory of the exciton fine structure induced by the long-range exchange interaction between the electron and the hole. The long-range exchange interaction is the driving force for the pseudospin or valley dynamics of excitons in semiconductors [38, 41, 43–46]. It can be calculated either quantum-mechanically by evaluating the matrix elements of the Coulomb potential over properly symmetrized two-particle Bloch functions or electrodynamically, taking into account the self-consistent action of the electric field induced by the exciton. The equivalence of these approaches has been established for two-dimensional semiconductors in Ref. [38]. The electrodynamical approach

has an advantage of being easily adapted for treatment of inhomogeneous structures such as the one studied here. Thus, we resort to the electrodynamical approach in this work.

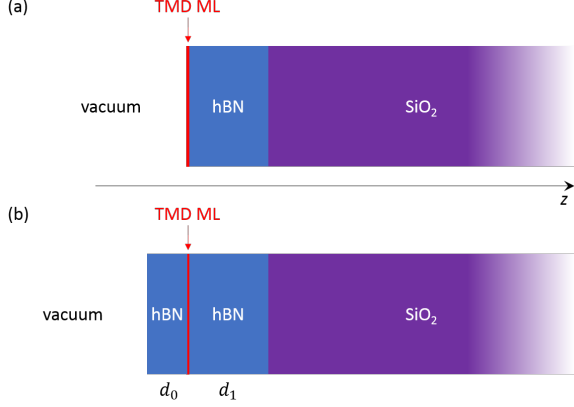


Figure 1. **Schematics of investigated van-der-Waals heterostructures.** (a) Structure without a cap hBN layer: TMD monolayer–hexagonal boron nitride (hBN)–silicon dioxide (SiO_2); (b) Structure with a cap hBN layer: hBN–TMD monolayer–bottom hBN layer– SiO_2 .

A. Structure and modes of electromagnetic field

We consider the van der Waals heterostructures based on transition metal dichalcogenides (TMD) monolayers (MLs) schematically depicted in Fig. 1. This corresponds to the typical stacking of the encapsulated TMD monolayers investigated in most of the experiments [47, 48]. Two types of structures are analysed: without and with cap hBN layer shown in Fig. 1 (a) and (b), respectively.

Within the framework of the electrodynamical approach the optically active exciton in TMD monolayer is considered as an in-plane electric dipole or current, oscillating at the optical transition frequency ω_0 , where

$$\hbar\omega_0 = E_g - E_B + \frac{\hbar^2 K^2}{2m}. \quad (1)$$

Here E_g is the band gap of the monolayer, E_B is the exciton binding energy, \mathbf{K} is the in-plane wavevector of the 2D exciton and m is its effective mass. In the relevant range of the wavevectors the dependence of ω_0 on \mathbf{K} can be disregarded. We also note that the variation of the environment, i.e., the thicknesses of the hBN layers, does not strongly affect the difference $E_g - E_B$, the spectral position of the exciton, while both band gap and exciton binding energy strongly depend on the screening [49, 50]. The induced current density can be written as [38]

$$\mathbf{j}(z) = \mathbf{J}\delta(z), \quad \mathbf{J} = \frac{c\omega_0}{2\pi\omega} \frac{i\Gamma_0}{\omega - \omega_0 + i\Gamma} \mathbf{E}_{\parallel}(z), \quad (2)$$

where \mathbf{J} is the 2D (surface) current density, Γ_0 and Γ are the radiative (into vacuum) and non-radiative decay rates of the exciton, the monolayer is assumed to be in the $z = 0$ plane, subscript parallel (\parallel) denotes the in-plane components of the field. In Eq. (2) \mathbf{E} is the electric field acting on the exciton, which includes both the external field and the field induced by the exciton, ω is the frequency of the field. The thickness of the monolayer is negligible as compared with the wavelength of light emitted by the exciton, that is why it is sufficient to use strictly two-dimensional model for the current density, Eq. (2).

In what follows we apply the uniaxial approximation for description of the excitonic states. In such a case the eigenmodes of the system, being the coupled modes of the exciton and electromagnetic field, can be described by the wavevector \mathbf{K} in the monolayer plane and polarization: the s -polarization corresponds to the $\mathbf{j}(z) \perp \mathbf{K}_{\parallel}$, this state is denoted as the transversal (T) exciton and the p -polarization corresponds to the $\mathbf{j}(z) \parallel \mathbf{K}_{\parallel}$, this state is denoted as the longitudinal (L) exciton.

The current $\mathbf{j}(z)$ in Eq. (2) is associated with the exciton induced electromagnetic field, which can propagate away from the monolayer or decay with the distance from the monolayer depending on the exciton wave vector. These regimes of field propagation are shown in Fig. 2. Top panel shows the light cones, i.e., the dispersion of free electromagnetic waves in the vacuum, SiO_2 , and hBN. In the case where the wavevector of the exciton lies in areas I or II,

$$K \leq \frac{\omega_0}{c} n_{\text{SiO}_2},$$

the exciton emits propagating waves, which cause its radiative decay. Interestingly, for $K \leq \omega_0/c$ the waves are propagating both to the vacuum and to the substrate (region I), while for $\omega_0/c \leq K \leq \omega_0 n_{\text{SiO}_2}/c$ the field decays into vacuum but propagates into SiO_2 . A self-consistent interaction of such exciton with the induced field leads to the difference of the decay rates for the longitudinal and transverse excitons [38]. The exciton with the wavevector outside the SiO_2 light cone, areas III and IV in Fig. 2, induces exponentially decaying waves (both into the vacuum and substrate). Here, its interaction with the self-consistent field results in the renormalization of the longitudinal and transverse excitons energies. We will mainly focus on the latter case where $K \geq \omega_0 n_{\text{SiO}_2}/c$, as for typical experimental parameters the states outside the light cones are mostly populated.

In order to find the exciton energy spectrum fine structure we have to self-consistently solve the Maxwell's equations

$$\text{rot } \mathbf{E} = -\frac{1}{c} \frac{\partial \mathbf{B}}{\partial t}, \quad (3a)$$

$$\text{rot } \mathbf{B} = \frac{1}{c} \frac{\partial \mathbf{D}}{\partial t} + \frac{4\pi}{c} \mathbf{j}(z), \quad (3b)$$

together with the Eq. (2) for the exciton-induced current and explicit expression for the electric induction

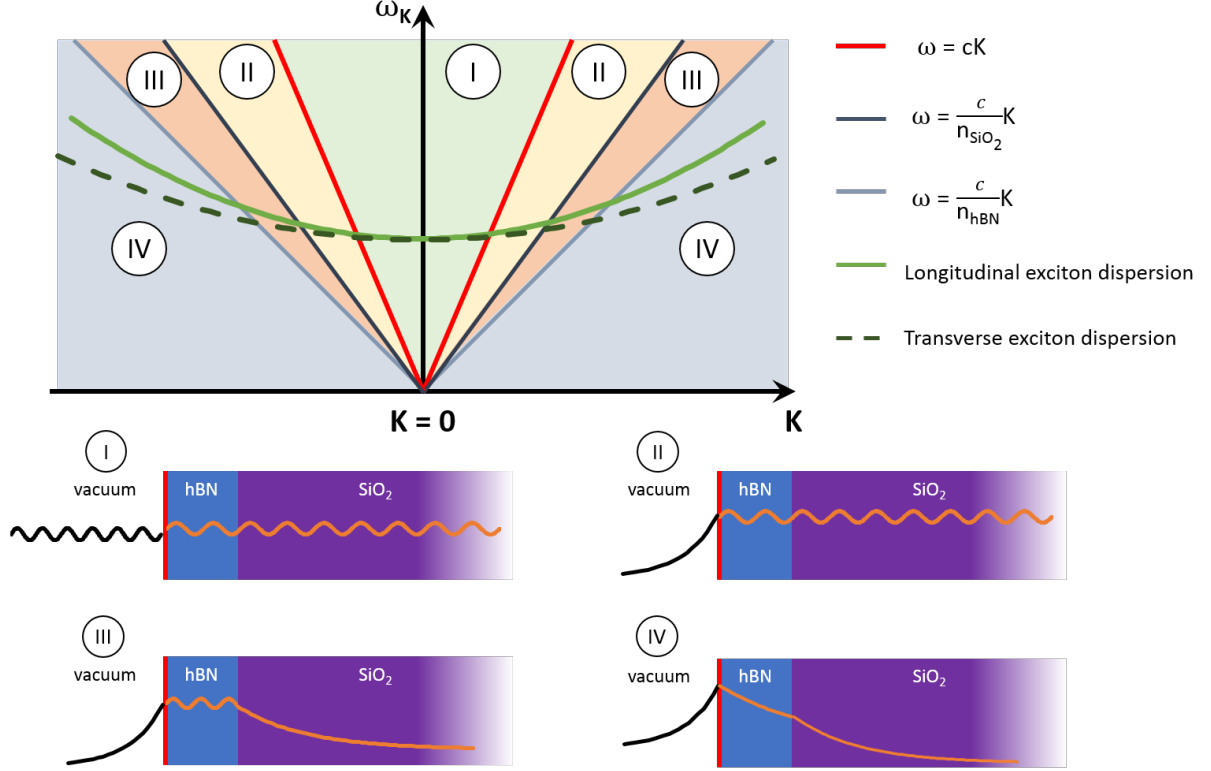


Figure 2. **Exciton dispersion and induced electromagnetic field.** Top panel: schematic illustration of longitudinal (L, solid curve) and transverse (T, dashed line) exciton energy spectra. $\mathbf{K} = 0$ point corresponds to center of the exciton Brillouin zone. Dispersion is shown not to scale. Four bottom panels (I) ... (IV) show schematics of the electromagnetic field distribution depending on area where the exciton wavevector lies. Wavy lines correspond to propagating waves $\propto \exp(ik_z|z|)$ induced by the exciton, decreasing curves correspond to decaying waves $\propto \exp(-\kappa_z|z|)$.

$\mathbf{D} = \varepsilon(z)\mathbf{E}$ with $\varepsilon(z)$ being the high-frequency (background) dielectric constant of the structure found disregarding excitonic effects. In this way, both the damping of the exciton and its energy renormalization due to the long-range exchange interaction can be derived automatically accounting for the screening and retardation effects [38, 51, 52]. To that end, it is convenient to include the current $\mathbf{j}(z)$ into the boundary condition for the in-plane components of magnetic field, namely,

$$\mathbf{B}_{\parallel}(z \rightarrow 0+) - \mathbf{B}_{\parallel}(z \rightarrow 0-) = \frac{4\pi}{c}[\mathbf{J} \times \mathbf{e}_z], \quad (4)$$

with \mathbf{e}_z being the unit vector along the normal to the ML. The remaining boundary conditions are the standard ones implying continuity of the in-plane components of \mathbf{E} and normal components of \mathbf{D} and \mathbf{B} at the interfaces. Below we present the results of solution of the Maxwell's equations and the analysis of the exciton fine structure.

B. Structure without a cap layer

It is instructive to analyze in detail the eigenstates of the exciton coupled with electromagnetic field in the simplest structure without a hBN cap layer, Fig. 1(a). Let us enumerate the layers of the structure: $i = 0$ is the vacuum ($z < 0$), $i = 1$ is the substrate hBN layer ($0 < z < d$) and $i = 2$ is the substrate SiO₂ ($z > d$). Inside each bulk layer we can write combining Eqs. (3):

$$\text{rot rot } \mathbf{E} = -\frac{\varepsilon_i}{c^2} \frac{\partial^2 \mathbf{E}}{\partial t^2}, \quad (5)$$

where ε_i is the dielectric permittivity of the i th layer. We seek the solution of Eq. (5) in the form of a plane wave in each layer

$$\mathbf{E}(\mathbf{r}) = \mathbf{E}^{(i)} e^{i\mathbf{k}_i \cdot \mathbf{r} - i\omega t}, \quad (6)$$

with $\mathbf{E}^{(i)}$ being its complex amplitude, \mathbf{k}_i is the light wavevector at the frequency of ω in the i th layer. Naturally, we find the absolute value of the wavevector $k_i = \sqrt{\varepsilon_i} \omega / c$. Without loss of generality, we set $\mathbf{k}_i = (0, k_{i,y}, k_{i,z})$ and take into account that its y -component, $k_{i,y} \equiv k_y$ remains constant in each dielectric layer because of the translational invariance of the system in the

(xy) plane. The z -component of the wavevector reads $k_{i,z} = \sqrt{\varepsilon_i k_z^2 + (\varepsilon_i - 1)k_y^2}$, with k_z being the wavevector component in the vacuum.

There are two eigenmodes of the electromagnetic field in each layer, namely, TE (or T-) mode and TM (or L-) mode, whose eigenvectors read

$$\mathbf{E}_{TE}^{(i)} = \begin{pmatrix} E_x^{(i)} \\ 0 \\ 0 \end{pmatrix}, \quad \text{and} \quad \mathbf{E}_{TM}^{(i)} = \begin{pmatrix} 0 \\ E_y^{(i)} \\ -\frac{k_y}{k_{i,z}} E_y^{(i)} \end{pmatrix}. \quad (7)$$

Correspondingly, the TE-mode couples with the transversal exciton and the TM-mode couples with the longitudinal exciton.

Further we have to construct the solution that satisfies the boundary conditions at the interfaces. Let us start with the TE-mode. We seek a solution for the electric field in a form (we assume the amplitude of the wave at $z \rightarrow -0$ wave equals to unity):

$$E_x = e^{ik_y y} \begin{cases} e^{\varkappa_{0,z} z}, & z < 0, \\ E_1 e^{-\varkappa_{1,z} z} + E_2 e^{\varkappa_{1,z} z}, & 0 < z < d, \\ E_3 e^{-\varkappa_{2,z}(z-d)}, & z > d. \end{cases} \quad (8)$$

Here we have selected the form of the fields relevant for the states outside the light cone ($k_y > \max_i \sqrt{\varepsilon_i}(\omega/c)$, region IV in Fig. 2) where $\varkappa_{i,z} = [k_y^2 - \varepsilon_i(\omega/c)^2]^{1/2} > 0$, which decay to the both sides of the structure. The boundary conditions of the continuity of the tangential components of the electric field read

$$E_1 + E_2 = 1, \quad (9a)$$

$$E_3 = E_1 e^{-\varkappa_{1,z} d} + E_2 e^{\varkappa_{1,z} d}. \quad (9b)$$

Expressing the tangential components of the magnetic field from Eq. (3a) and making use of the boundary condition (4) at $z = 0$ and the continuity condition at $z = d$ we have

$$\varkappa_{1,z}(E_1 - E_2) + \varkappa_{0,z} = \frac{(\omega/c)^2}{\omega_0/c} \frac{2\Gamma_0}{\omega_0 - \omega - i\Gamma}, \quad (10a)$$

$$\varkappa_{2,z}E_3 = \varkappa_{1,z}E_1 e^{-\varkappa_{1,z} d} - \varkappa_{1,z}E_2 e^{\varkappa_{1,z} d}. \quad (10b)$$

The boundary conditions Eqs. (9) and (10) represent the set of four equations for three amplitudes E_1, E_2, E_3 . Its compatibility condition allows us to find the renormalized energies of excitons due to the light-matter interaction, i.e., taking into account the long-range exchange interaction. As we are looking for the relatively small renormalizations of the exciton energy, where $|\hbar\omega - \hbar\omega_0| \ll \hbar\omega_0$, it is accurate to replace ω with ω_0 everywhere except for the denominator in the right side of Eq. (10a). As a result, combining Eqs. (9) and (10), we find for the eigenfrequency $\omega_T \equiv \omega$ of the transversal exciton:

$$\frac{\omega_T - \omega_0}{\Gamma_0} = -\frac{2\zeta}{s_0 - s_1 + \frac{2s_1(s_1+s_2)}{s_1+s_2+(s_1-s_2)e^{-2as_1}}}. \quad (11a)$$

Here the following notations are introduced

$$\zeta = \frac{1}{K} \frac{\omega_0}{c}, \quad s_i = \sqrt{1 - \varepsilon_i \zeta^2}, \quad a = Kd. \quad (11b)$$

Analogous calculation for the TM-polarized mode yields the eigenfrequency ω_L of the longitudinal exciton:

$$\begin{aligned} & \frac{\omega_L - \omega_0}{\Gamma_0} \\ &= \frac{2}{\frac{\zeta}{s_0} + \frac{\varepsilon_1 \zeta}{s_1} \left(\frac{2(\varepsilon_2 s_1 + \varepsilon_1 s_2)}{\varepsilon_1 s_2 + \varepsilon_2 s_1 + (\varepsilon_1 s_2 - \varepsilon_2 s_1)e^{-2as_1}} - 1 \right)}. \end{aligned} \quad (11c)$$

Equations (11a) and (11c) describe the dispersion of the transversal and longitudinal excitons in the van der Waals heterostructure without a cap layer, Fig. 1(a).

C. Effect of the cap hBN layer

Now we consider a van der Waals heterostructure capped with a hBN layer as the ones used in most of the experiments, Fig. 1(b). Explicit expression for exciton energies with account for the exchange interaction can be found by solving the set of Maxwell's equations (3) with appropriate boundary conditions. As the solution is completely analogous to that presented above in Sec. II B for an uncapped structure and quite lengthy, we just give here the results for the radiative doublet eigenfrequencies:

$$\frac{\omega_T - \omega_0}{\Gamma_0} = -\frac{\zeta}{\sqrt{1 - \varepsilon_1 \zeta^2}} \frac{(1 - r_{1,s} \xi_0)(1 + r_{b,s} \xi_1)}{1 + r_{1,s} r_{b,s} \xi_0 \xi_1}, \quad (12a)$$

$$\frac{\omega_L - \omega_0}{\Gamma_0} = \frac{\sqrt{1 - \varepsilon_1 \zeta^2}}{\varepsilon_1 \zeta} \frac{(1 - r_{1,p} \xi_0)(1 + r_{b,p} \xi_1)}{1 + r_{1,p} r_{b,p} \xi_0 \xi_1}. \quad (12b)$$

Here

$$\xi_i = \exp \left[-2d_i \frac{\omega_0}{c} \frac{\sqrt{1 - \varepsilon_i \zeta^2}}{\zeta} \right], \quad (13)$$

d_i are the thicknesses of the cap, $i = 0$, and the substrate, $i = 1$, hBN layers; $r_{1,\alpha}$ is the reflection coefficient of $\alpha = s, p$ -polarized light from vacuum-hBN interface, expressed using Fresnel's equations [53]:

$$r_{1,s} = \frac{1 - \sqrt{\frac{1 - \varepsilon_1 \zeta^2}{1 - \zeta^2}}}{1 + \sqrt{\frac{1 - \varepsilon_1 \zeta^2}{1 - \zeta^2}}}, \quad r_{1,p} = \frac{\varepsilon_1 - \sqrt{\frac{1 - \varepsilon_1 \zeta^2}{1 - \zeta^2}}}{\varepsilon_1 + \sqrt{\frac{1 - \varepsilon_1 \zeta^2}{1 - \zeta^2}}}; \quad (14)$$

and $r_{b,\alpha}$ is the reflection coefficient from the hBN-SiO₂ interface:

$$r_{b,s} = \frac{1 - \sqrt{\frac{1 - \varepsilon_2 \zeta^2}{1 - \varepsilon_1 \zeta^2}}}{1 + \sqrt{\frac{1 - \varepsilon_2 \zeta^2}{1 - \varepsilon_1 \zeta^2}}}, \quad r_{b,p} = \frac{\frac{\varepsilon_2}{\varepsilon_1} - \sqrt{\frac{1 - \varepsilon_2 \zeta^2}{1 - \varepsilon_1 \zeta^2}}}{\frac{\varepsilon_2}{\varepsilon_1} + \sqrt{\frac{1 - \varepsilon_2 \zeta^2}{1 - \varepsilon_1 \zeta^2}}}. \quad (15)$$

As expected, at $d_0 = 0$ Eqs. (12) are identical to Eqs. (11).

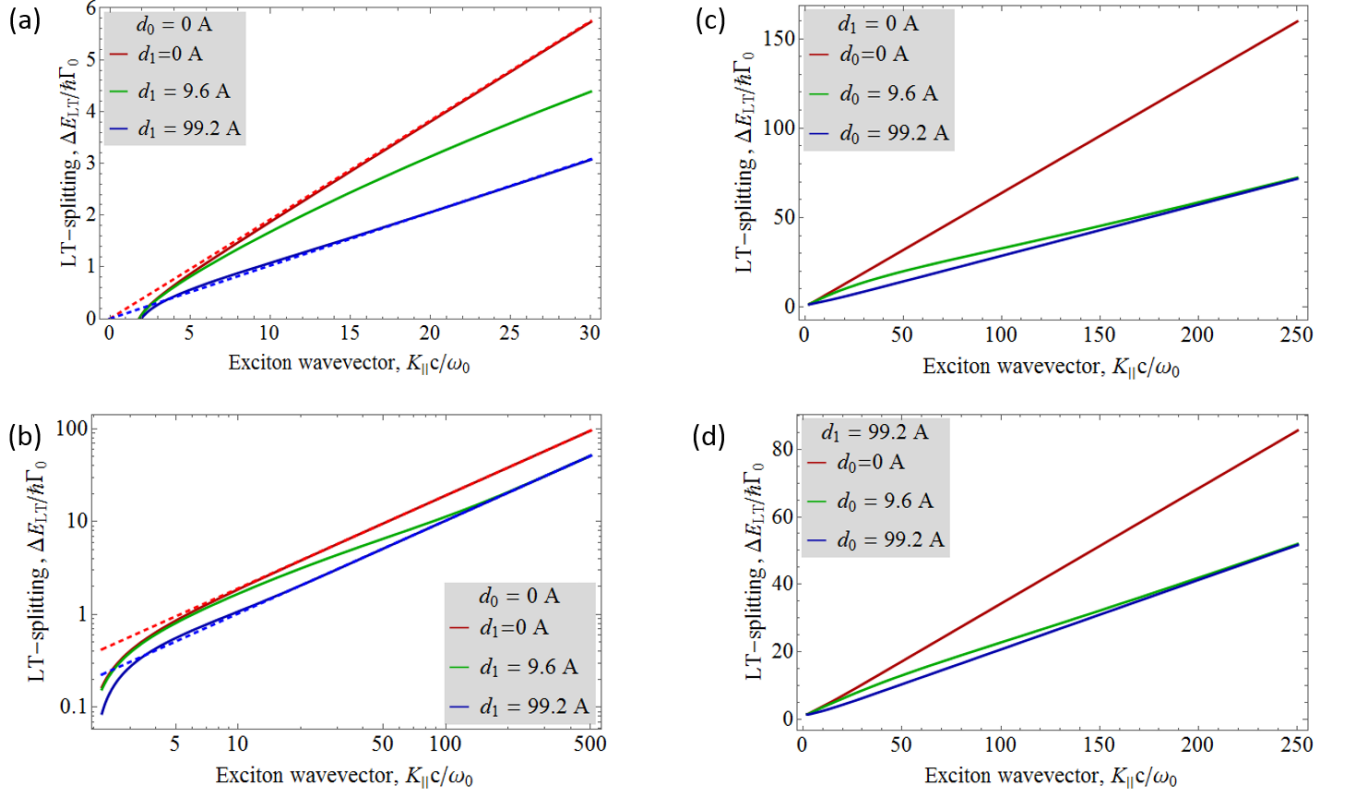


Figure 3. **Exciton fine structure splitting.** LT-splitting as a function of the exciton wavevector in the structure without a cap hBN layer ($d_0 = 0$) in linear scale (a), log-log scale (b); and in the structures without a substrate hBN layer ($d_1 = 0$) (c), and with the substrate hBN layer of finite thickness ($d_1 = 99.2$ Å) (d), while the cap hBN layer thickness being varied. Dashed lines illustrate asymptotics, Eq. (17): blue dashed line corresponds to $d_{\text{hBN}} \neq 0$ asymptotics, red dashed line corresponds to $d_{\text{hBN}} = 0$. Parameters of the calculation are: $\varepsilon_{\text{hBN}} = 4.84$ is the hBN permittivity, $\varepsilon_{\text{SiO}_2} = 2.13$ is the SiO_2 permittivity, $\omega_0/c = 981745 \text{ cm}^{-1}$ (which roughly corresponds to MoS_2 ML), $\hbar\Gamma_0 = 0.3 \text{ meV}$.

D. Effect of the hBN layers on the exciton fine structure

In agreement with the symmetry arguments we have demonstrated microscopically that the exciton eigenstates in TMD monolayers are the L- and T-polarized states with the microscopic dipole moment of the exciton (or microscopic current) oriented parallel and perpendicular to its in-plane wavevector. Equations (11) and (12) are valid for arbitrary values of the exciton in-plane wavevector K , including both the states inside and outside of the light cone. In what follows, however, we will mostly consider the states outside of the light cone, region IV in Fig. 2 where the induced field decays with the distance from the monolayer and $\varkappa_{i,z} \in \mathbb{R}$. Thus, the parameters s_i in Eq. (11b) and ξ_i in Eq. (13) are real. As a result, $\omega_{L,T}$ are real. In this case, as expected, the coupling with the induced electromagnetic field, i.e., the long-range exchange interaction between the electron and hole, produces the splitting of the L- and T-exciton energies. Note that for the states inside the light cone the eigenfrequencies ω_L and ω_T contain imaginary parts

as well being responsible for the radiative damping of excitons, see Refs. [15, 38] for details.

Figure 3 shows the results for the exciton LT-splitting,

$$\Delta E_{LT} = \hbar\omega_L - \hbar\omega_T, \quad (16)$$

calculated as function of the exciton wavevector K for different thicknesses of the hBN layers. Panels (a) and (b) show the results for the absent cap layer ($d_0 = 0$), while panels (c) and (d) show the results for the structure with the cap layer. Solid lines are calculated after Eqs. (11) and (12), while dotted lines are the analytical asymptotics, Eqs. (17) and (19), see below.

Let us first analyze the LT-splitting as a function of the exciton wavevector K . At small wavevectors $K \lesssim \omega_0/c$ the ΔE_{LT} is a strongly non-linear function of K and its real part vanishes for the states within the light cone.¹ For sufficiently large exciton wave vectors, $K \gg \omega_0/c$, the

¹ In the region II there are both real and imaginary parts of $\omega_{L,T}$ due to the leaky waveguide-like modes in the structure.

parameter $\zeta \sim K_{\parallel}^{-1} \rightarrow 0$. It follows then from Eqs. (11a) and (12a) that, $\omega_T - \omega_0 \propto \zeta$. Thus, for large wave vectors the energy of the transversal exciton is almost not renormalized. Conversely, one can see from the formulas (11c) and (12b) that $\omega_L - \omega_0 \sim \zeta^{-1} \sim K_{\parallel}$. Therefore, the longitudinal exciton energy renormalization and the LT-splitting of the radiative doublet for large enough exciton wavevectors are equal and linear in K .

The asymptotic behavior of the exciton LT-splitting at $K \gg \omega_0/c$ can be recast as

$$\Delta E_{LT} = \frac{\hbar \Gamma_0}{\varepsilon_{\text{eff}}(K, d_0, d_1)} \frac{cK}{\omega_0}, \quad (17)$$

with the effective dielectric constant $\varepsilon_{\text{eff}}(K, d_0, d_1)$ being a function of the exciton wavevector and the structure geometry. In the structures with negligible cap layer thickness, $Kd_0 \ll 1$

$$\varepsilon_{\text{eff}}(K, 0, d_1) = \frac{1}{2} \times \begin{cases} 1 + \varepsilon_{\text{SiO}_2}, & Kd_1 \ll 1, \\ 1 + \varepsilon_{\text{hBN}}, & Kd_1 \gg 1. \end{cases} \quad (18)$$

Physical sense of this expression is as follows. If there is no substrate hBN layer at all or hBN layer thickness is negligible, i.e., $Kd_1 \ll 1$, the field decays mainly into the vacuum and SiO₂ substrate. As a result, an effective permittivity of such structure is the average of the permittivities of vacuum and SiO₂. When the hBN layer thickness is sufficiently large, $Kd_1 \gg 1$, the electric field induced by the exciton decays into the hBN layer and there is almost no field in SiO₂. So effective permittivity contains that of hBN instead SiO₂.

This behavior is illustrated in Fig. 3(a,b). The curve corresponding to the intermediate thickness of the hBN substrate layer, $d_1 = 9.6 \text{ \AA}$ (i.e., 3 monoatomic layers of hBN)² for small wave vectors is close to zero thickness asymptotics, and for large ones it goes over to the thick hBN layer asymptotics. The behavior of the ΔE_{LT} for sufficiently large K is very well described by the linear law (17) with the effective dielectric constant ε_{eff} given by Eq. (18).

Similar results take place in the structures with the cap layer. Assuming that its thickness is sufficiently large, $Kd_0 \gg 1$, we have Eq. (17) with the effective permittivity in the form

$$\varepsilon_{\text{eff}}(K, \infty, d_1) = \frac{1}{2} \times \begin{cases} \varepsilon_{\text{hBN}} + \varepsilon_{\text{SiO}_2}, & Kd_1 \ll 1, \\ 2\varepsilon_{\text{hBN}}, & Kd_1 \gg 1. \end{cases} \quad (19)$$

This expression is analogous to Eq. (17) except that instead of the vacuum permittivity, which is equal to 1, the hBN permittivity enters ε_{eff} in Eq. (19). This is because for large wavevectors the exciton-induced field is mostly

concentrated in the cap hBN layer and does not reach vacuum. Corresponding behavior is illustrated in Fig. 3 panels (c) and (d).

In contrast to the case of the environment effect on the exciton radiative decay rate, where the decay rate shows pronounced oscillations as a function of the hBN layer thickness [15], here the hBN layer thickness enters $\omega_{L,T}$ through the damped exponential function. The difference is because the LT-splitting of the exciton takes place for the states outside the light cone, where the exciton-induced field decays exponentially to both sides of the monolayer. It is seen from Eqs. (11), (12) and asymptotic expressions (17), (18), and (19) that increasing the hBN thickness results in a reduction of the LT splitting.

One can say that the long-range exchange interaction is screened by the presence of the hBN layers. Calculations presented in Fig. 3 confirm this result.

III. CONTROL OF THE EXCITON SPIN/VALLEY DYNAMICS

In this section we present the model description of the exciton valley dynamics. We present and solve the kinetic equation for the exciton density matrix and analyze the impact of the environment in the van der Waals heterostructure on the valley depolarization.

A. Kinetic equation and its solution

We describe valley dynamics of excitons in monolayer semiconductors within the pseudospin density matrix approach [38–40, 43]. We introduce the 2×2 density matrix

$$\varrho_{\mathbf{K}} = n_{\mathbf{K}} + \boldsymbol{\sigma} \cdot \mathbf{s}_{\mathbf{K}}, \quad (20)$$

where $n_{\mathbf{K}}$ is the average occupancy of the orbital state \mathbf{K} , i.e., $n_{\mathbf{K}}$ is the exciton distribution function, and $\mathbf{s}_{\mathbf{K}}$ is the pseudospin distribution function, with $\mathbf{s}_{\mathbf{K},z}$ component describing the valley polarization or circular polarization of excitons, while the in-plane components $\mathbf{s}_{\mathbf{K},x}, \mathbf{s}_{\mathbf{K},y}$ describe the valley coherence or exciton alignment/linear polarization. In Eq. (20), $\boldsymbol{\sigma} = (\sigma_x, \sigma_y, \sigma_z)$ is the vector composed of the 2×2 Pauli matrices; the unit matrix in this notation is omitted.

In the basis of circularly polarized components, the Hamiltonian of the exciton LT-splitting takes the form

$$\begin{aligned} \mathcal{H}(\mathbf{K}) &= \frac{\Delta E_{LT}}{2} [\sigma_x \cos(2\varphi_{\mathbf{K}}) + \sigma_y \sin(2\varphi_{\mathbf{K}})] \\ &= \frac{\hbar}{2} (\boldsymbol{\Omega}_{\mathbf{K}} \boldsymbol{\sigma}), \end{aligned} \quad (21)$$

where the vector

$$\boldsymbol{\Omega}_{\mathbf{K}} = (\Delta E_{LT}/\hbar) [\cos(2\varphi_{\mathbf{K}}), \sin(2\varphi_{\mathbf{K}}), 0], \quad (22)$$

plays a role of the exciton pseudospin precession frequency in the effective field caused by the LT-splitting.

² The thickness of monoatomic hexagonal boron nitride equals to 3.2 Å.

Within the relaxation time approximation the kinetic equation for the exciton pseudospin distribution takes the form [39] [cf. Ref. [54]]

$$\frac{\partial \mathbf{s}_K}{\partial t} + \mathbf{s}_K \times \boldsymbol{\Omega}_K + \frac{\mathbf{s}_K - \bar{\mathbf{s}}_K}{\tau} = \mathbf{g}_K. \quad (23)$$

Here τ is the exciton relaxation time, $\bar{\mathbf{s}}_K = (2\pi)^{-1} \int_0^{2\pi} \mathbf{s}_K d\varphi_K$ is the angular average of the exciton pseudospin, and \mathbf{g}_K is the pseudospin generation rate.

In what follows we consider the simplest and experimentally relevant situation where the valley-polarized excitons are created by a short circularly polarized light pulse. We perform further calculations in the approximation of the fast exciton energy relaxation: we suppose that after an ensemble of excitons is excited by optical pulse, the Boltzmann energy distribution sets in a short time by valley conserving processes. Thus we employ the following initial condition for Eq. (23) and set $\mathbf{g}_K = 0$:

$$s_{z,K}(t=0) = s_0 \frac{2\pi\hbar^2}{m\mathcal{S}} \frac{\exp(-\epsilon/T)}{T}. \quad (24)$$

Here $\epsilon = \hbar^2 K^2/2m$ is the exciton kinetic energy, T is the temperature measured in energy units ($k_B \equiv 1$), \mathcal{S} is the normalization area, and $s_0 = \sum_K s_{z,K}(t=0)$ is the average spin at $t=0$. Since our aim is to study the effect of the dielectric environment on the exciton valley dynamics we abstain from the description and analysis of the exciton formation processes and details of its energy relaxation, cf. Refs. [32, 36, 55, 56]. We also stress that the condition $T\tau/\hbar \gg 1$ is fulfilled, otherwise the corrections to the kinetic equation related, e.g., to the weak localization effects should be taken into account [57].

Making use of the explicit form of $\boldsymbol{\Omega}_K$ one arrives at the following equation for the $\bar{s}_{z,K}$ [58]:

$$\left(\frac{\partial}{\partial t} + \frac{1}{\tau} \right) \frac{\partial}{\partial t} \bar{s}_{z,K} + \Omega_K^2 \bar{s}_{z,K} = 0, \quad (25)$$

where we took into account that $s_{z,K} = \bar{s}_{z,K}$. In agreement with Refs. [59, 60] we obtain the expression for valley polarization dynamics:

$$\bar{s}_{z,K} = e^{-\frac{t}{2\tau}} \left(\frac{\sinh \frac{qt}{2\tau}}{q} + \cosh \frac{qt}{2\tau} \right) s_{z,K}(t=0), \quad (26)$$

where $q \equiv q(\epsilon) = \sqrt{1 - (2\Delta E_{LT}\tau/\hbar)^2}$. Ultimately, we arrive at the following expression for valley polarization dynamics of excitons:

$$\begin{aligned} S_z(t) &= \sum_K \bar{s}_{z,K} \\ &= s_0 e^{-\frac{t}{2\tau}} \int_0^\infty \frac{e^{-\frac{\epsilon}{T}}}{T} \left(\frac{\sinh \frac{q(\epsilon)t}{2\tau}}{q(\epsilon)} + \cosh \frac{q(\epsilon)t}{2\tau} \right) d\epsilon. \end{aligned} \quad (27)$$

Strictly speaking, the integral over energy in Eq. (27) should be cut-off at small energies $\epsilon^* \sim \hbar^2 \omega_0^2/(2mc^2)$, i.e., for the states within the light cone. Estimates show that this cut-off is unimportant at reasonable temperatures $T \gtrsim 1$ K.

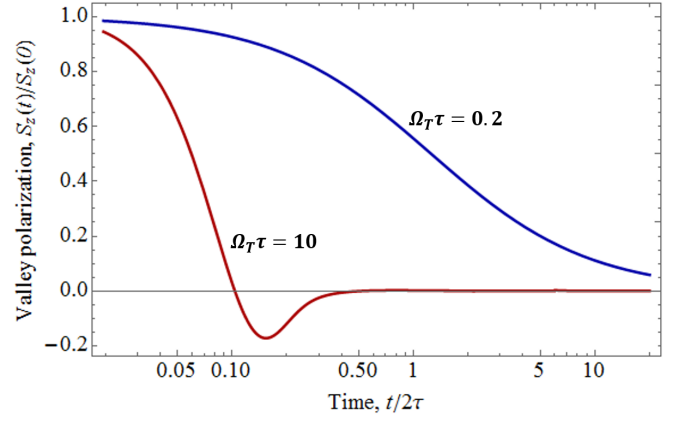


Figure 4. **Exciton spin/valley dynamics in limiting cases.** Blue curve illustrates characteristic valley polarization dynamics in collision-dominated regime ($\Omega_T \tau \ll 1$), red one corresponds to the rare scattering regime ($\Omega_T \tau \gg 1$).

B. Exciton spin/valley dynamics in limiting cases

Before turning to the numerical results, let us deduce analytical asymptotics of the integral (27) for important limiting cases. Characteristic – average – energy of the exciton ensemble is the temperature T , which determines a typical value of the thermal wavevector $K_T = \sqrt{2mT}/\hbar$ and, accordingly, the typical pseudospin precession frequency $\Omega_T \equiv \Omega_{K_T}$. We consider the behaviour of the integral (27) and spin dynamics in the two important cases, where the pseudospin precession frequency is either much smaller than the scattering rate τ^{-1}

$$\Omega_T \tau \ll 1, \quad (28a)$$

or much larger than τ^{-1} :

$$\Omega_T \tau \gg 1. \quad (28b)$$

In both cases simple analytical expressions describing the spin dynamics are derived.

In the first situation where the scattering acts are frequent, Eq. (28a), we use the asymptotics $q(\epsilon) \approx 1 - 2(\Delta E_{LT}\tau/\hbar)^2$, and obtain:

$$S_z(t) = s_0 \int_0^\infty \frac{e^{-\frac{\epsilon}{T}}}{T} \exp[-(\Delta E_{LT}/\hbar)^2 \tau t] d\epsilon. \quad (29)$$

The energy dependence of the subintegral expression results from both the Boltzmann exponent $\exp(-\epsilon/T)$ and the wavevector dependence on the ΔE_{LT} . The latter can be written, in accordance with Eq. (17), as

$$\Delta E_{LT} = \hbar\beta\sqrt{\epsilon}, \quad \beta = \sqrt{\frac{2mc^2}{\omega_0^2}} \frac{\Gamma_0}{\epsilon_{\text{eff}}(K_T, d_0, d_1)}. \quad (30)$$

In derivation of Eq. (30) we disregarded K -dependence of the effective permittivity assuming that relevant

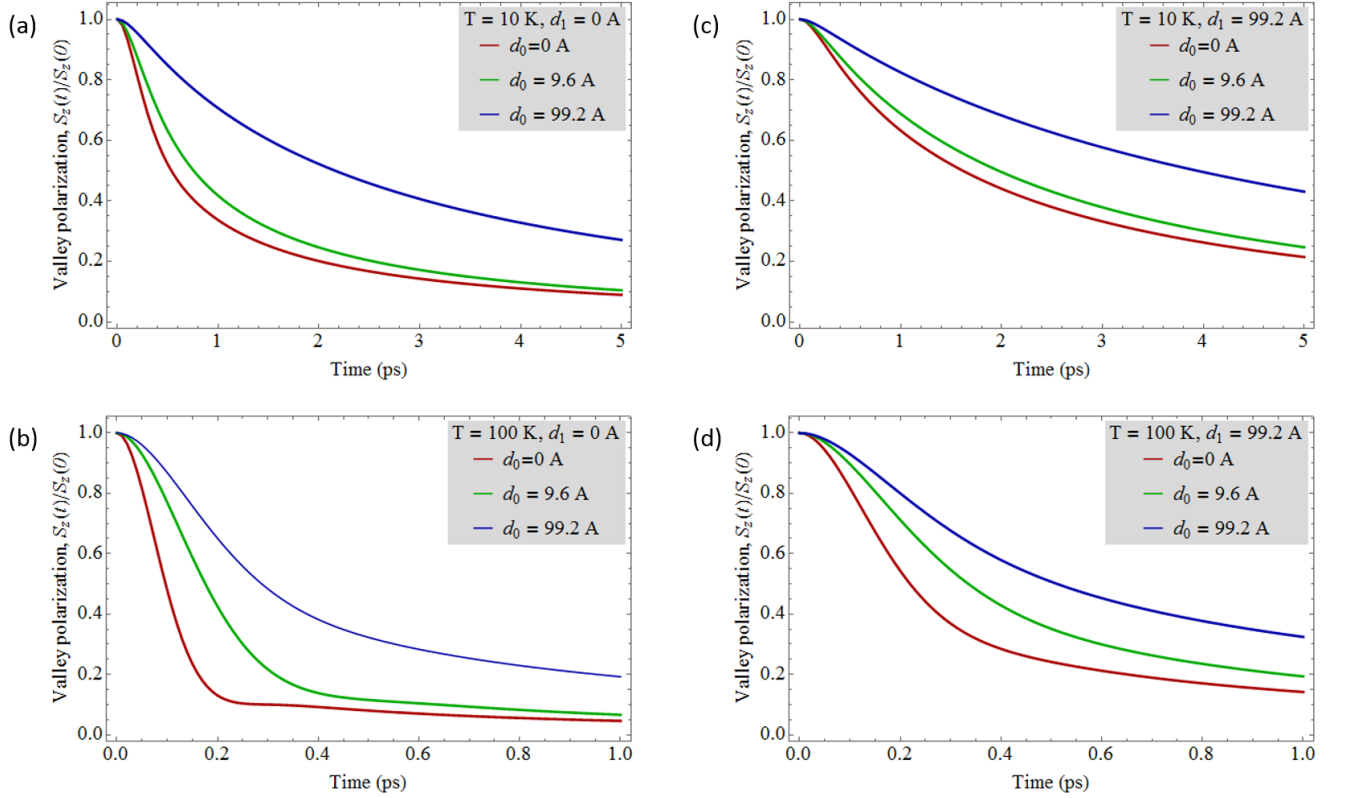


Figure 5. **Valley polarization dynamics for different structure parameters.** Panels (a) and (b) correspond to the absent substrate hBN layer ($d_1 = 0$) and two temperatures $T = 10$ K and 100 K, respectively. Panels (c) and (d) correspond to the structure with sufficiently thick substrate hBN layer ($d_1 = 99.2$ Å) and two temperatures $T = 10$ K and 100 K. Different curves show the valley polarization dynamics for different top hBN layer thicknesses. Parameters of the calculations are the same as in Fig. 3 and the scattering time $\tau = 0.1$ ps is assumed to be temperature and energy independent.

wavevectors are sufficiently large. The resulting integral is readily evaluated as

$$S_z(t) = \frac{s_0}{1 + T\beta^2\tau t}. \quad (31)$$

The exciton valley depolarization rate is given by

$$\frac{1}{\tau_v} \equiv \beta^2 T \tau \sim \Omega_T^2 \tau, \quad (32)$$

in accordance with the general result in the collision-dominated regime [38, 54, 61]. Interestingly, the decay is slow with $S_z(t) \propto t^{-1}$ at $t \gg \tau_v$. This $1/t$ ‘tail’ is a result of neglected energy relaxation processes. If the exciton energy relaxation time τ_ϵ is sufficiently short as compared with the valley depolarization time, $\tau_\epsilon \ll \tau_v$, but simultaneously sufficiently long compared to the momentum relaxation time, $\tau_\epsilon \gg \tau$, then the exciton ensemble is characterized by a single relaxation rate τ_v^{-1} in Eq. (32)

and, instead of Eqs. (29) and (31) we obtain

$$S_z(t) = s_0 \exp \left[- \int_0^\infty \frac{e^{-\frac{\epsilon}{T}}}{T} (\Delta E_{LT}/\hbar)^2 \tau t d\epsilon \right] = s_0 \exp(-t/\tau_v). \quad (33)$$

In this situation standard exponential decay law of the valley polarization is recovered.

Now we turn to the limit of rare scattering events [60, 62], Eq. (28b) we have $q(\epsilon) \approx 2i\Delta E_{LT}\tau/\hbar$, and it follows from Eqs. (27) and (30) that [cf. Ref. [39]]

$$S_z(t) = s_0 e^{-\frac{t}{2\tau}} \int_0^\infty \frac{e^{-\frac{\epsilon}{T}}}{T} \cos(\beta\sqrt{\epsilon}t) d\epsilon = s_0 e^{-\frac{t}{2\tau}} \left[1 - \sqrt{T}\beta t F\left(\frac{\sqrt{T}\beta t}{2}\right) \right], \quad (34)$$

where $F(x) = \exp(-x^2) \int_0^x \exp(t^2) dt$ is the Dawson function. In this regime the valley polarization decays mainly due to the spread of the pseudospin precession frequencies with the characteristic rate $\beta\sqrt{T} \sim \Omega_T$. The scat-

tering breaks phase of the pseudospin precession and results in the additional exponential decay with the rate $1/(2\tau)$ [60].

From asymptotics (31) and (34) one can see, that in the case $\Omega_T\tau \ll 1$ we expect slow monotonous relaxation of the exciton valley polarization as shown in Fig. 4. If, by contrast, $\Omega_T\tau \gg 1$, we expect fast decoherence with a characteristic minima, see Fig. 4.

C. Numerical results and discussion

Figure 5 shows the valley polarization dynamics calculated numerically after Eq. (27) for various parameters of the structure and two characteristic temperatures $T = 10$ K and 100 K. Panels (a) and (b) show the dynamics for the structure without a substrate hBN layer, while panels (c) and (d) demonstrate the dynamics in the structures with the substrate layer. Overall behavior of the valley polarization $S_z(t)$ is intermediate between the asymptotics shown in Fig. 4. Figure 5 demonstrates clearly that the exciton valley relaxation time can be controlled by the dielectric environment engineering.

For a fixed hBN layers thicknesses the valley depolarization rate increases with increase of the temperature. This is because at a higher temperature the characteristic pseudospin precession frequency Ω_T increases. It is in agreement with experimental data [61].

An increase of the hBN layers thicknesses results, as discussed in Sec. II, in the effective screening of the exchange interaction and, correspondingly, in suppression of the exciton LT-splitting. As a result, at a fixed thickness of the substrate hBN layer d_1 , an increase in the cap layer thickness d_0 slows-down the valley depolarization, compare red, green and blue curves in the panels. Similarly, an increase in d_1 at a fixed d_0 slows down depolarization as well, compare Fig. 5 (a) with (c) and (b) with (d).

Calculations show that the spin dynamics is fastest for the structure without hBN, $d_0 = d_1 = 0$. At $T = 100$ K the product $\Omega_T\tau$ exceeds unity and slightly non-monotonic behavior of the red curve in Fig. 5(b) is seen. Overall, the modulation of the valley depolarization time for different system parameters is significant, compare red and blue lines in Fig. 5(a).

The predictions for the control of the exciton spin/valley polarization lifetime are summarized in Fig. 6 where the dependence of the τ_v on the cap hBN layer thickness is presented for the structure shown in Fig. 1(b) for different substrate hBN thicknesses d_1 . We determine the spin/valley depolarization time τ_v from the condition $S_z(\tau_v)/S_z(0) = 1/e$, i.e., it corresponds to the decay by $e \approx 2.718$. One can see that for a fixed d_1 the depolarization time increases with increasing d_0 and, similarly, for a fixed d_0 the depolarization time increases with increasing d_1 . This is because of the effective screening of the electron-hole long-range exchange interaction. The significant modulation of τ_v is seen. Note that signifi-

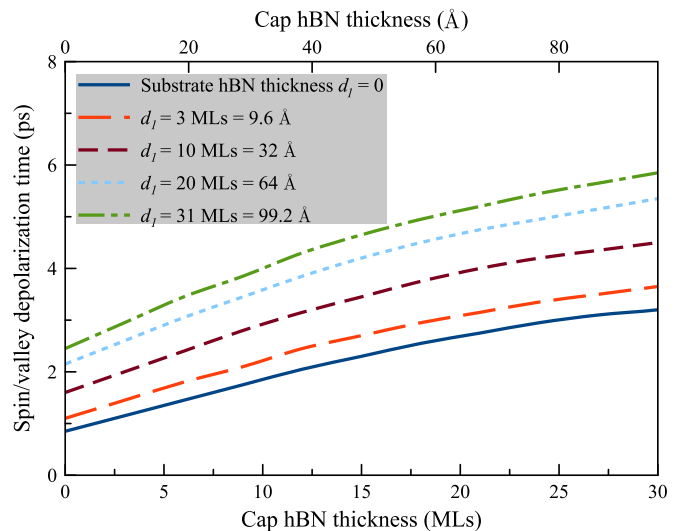


Figure 6. **Controlling the exciton spin/valley depolarization.** Exciton spin/valley polarization lifetime τ_v as a function of the top hBN layer thickness d_0 for the structure shown in Fig. 1(b) at calculated for different values of the substrate hBN thickness d_1 (different curves). Temperature $T = 10$ K, scattering time $\tau = 0.1$ ps. The depolarization time τ_v is defined as $S_z(\tau_v)/S_z(0) = 1/e$.

cant variation of τ_v is observed for very small variations (\sim nm) of the hBN thickness. Comparing the structures without encapsulation $d_1 = d_0 = 0$ and structures with sufficiently thick encapsulation, 30 MLs of hBN for both the cap and substrate layers one can see that the variation of τ_v by a factor $\gtrsim 5$ is possible.

IV. CONCLUSION

We have studied the effect of the dielectric environment of the atomically thin semiconductor on the exciton fine structure and its valley depolarization in van der Waals heterostructures based on transition metal dichalcogenide monolayers encapsulated into hexagonal boron nitride. The microscopic theory of the exciton fine structure has been developed within the electrodynamical approach where the long-range exchange interaction naturally appears as a result of the exciton coupling with the induced electromagnetic field. The valley dynamics has been studied within the kinetic equation approach for the pseudospin density matrix.

We have demonstrated that the encapsulation of the monolayer into hBN effectively screens the long-range exchange interaction and results in a slow-down of the valley depolarization. While the radiative decay of excitons in monolayer semiconductors and the electron-hole long-range exchange interaction have the same physical origin, related to the self-consistent interaction of the exciton with its electromagnetic field, their dependence on the boron nitride layer thickness is different. In the radiative recombination process, the excitonic states within

the light cone are involved. Those states induce propagating electromagnetic field which oscillates in space. As a result, the radiative decay rate shows oscillations as a function of the hBN thickness [15]. In the studied case of the long-range exchange interaction, the excitons are outside of the light cone and they induce decaying in space electromagnetic field. It gives rise to a monotonic dependence of the longitudinal-transverse splitting of excitonic states as a function of the hBN thickness.

Our calculations demonstrate a significant, up to five-fold, variation of the valley depolarization in hBN-based van der Waals heterostructures. Our results open up the possibilities to control the exciton valley dynamics by ap-

propriately tailoring the electrodynamic environment of the monolayer.

ACKNOWLEDGMENTS

We thank M.A. Semina for valuable discussions. This work was partially supported by the Russian Science Foundation, project No. 19-12-00051, ANR 2D-vdW-Spin, MagicValley, and Vallex, as well as the French-Russian IRP PHYNICS. A.I.P. was supported in part by the Foundation for the Advancement of Theoretical Physics and Mathematics “BASIS”.

-
- [1] A. K. Geim and I. V. Grigorieva, “Van der Waals heterostructures,” *Nature* **499**, 419–425 (2013).
 - [2] Sheneve Z. Butler, Shawna M. Hollen, Linyou Cao, Yi Cui, Jay A. Gupta, Humberto R. Gutiérrez, Tony F. Heinz, Seung Sae Hong, Jiaying Huang, Ariel F. Ismach, Ezekiel Johnston-Halperin, Masaru Kuno, Vladimir V. Plashnitsa, Richard D. Robinson, Rodney S. Ruoff, Sayeef Salahuddin, Jie Shan, Li Shi, Michael G. Spencer, Mauricio Terrones, Wolfgang Windl, and Joshua E. Goldberger, “Progress, challenges, and opportunities in two-dimensional materials beyond graphene,” *ACS Nano* **7**, 2898–2926 (2013).
 - [3] Andrea Splendiani, Liang Sun, Yuanbo Zhang, Tianshu Li, Jonghwan Kim, Chi-Yung Chim, Giulia Galli, and Feng Wang, “Emerging photoluminescence in monolayer MoS₂,” *Nano Letters* **10**, 1271 (2010).
 - [4] Kin Fai Mak, Changgu Lee, James Hone, Jie Shan, and Tony F. Heinz, “Atomically thin MoS₂: A new direct-gap semiconductor,” *Phys. Rev. Lett.* **105**, 136805 (2010).
 - [5] Keliang He, Nardeep Kumar, Liang Zhao, Zefang Wang, Kin Fai Mak, Hui Zhao, and Jie Shan, “Tightly bound excitons in monolayer WSe₂,” *Phys. Rev. Lett.* **113**, 026803 (2014).
 - [6] Alexey Chernikov, Timothy C. Berkelbach, Heather M. Hill, Albert Rigosi, Yilei Li, Ozgur Burak Aslan, David R. Reichman, Mark S. Hybertsen, and Tony F. Heinz, “Exciton binding energy and nonhydrogenic Rydberg series in monolayer WS₂,” *Phys. Rev. Lett.* **113**, 076802 (2014).
 - [7] Hongyi Yu, Xiaodong Cui, Xiaodong Xu, and Wang Yao, “Valley excitons in two-dimensional semiconductors,” *National Science Review* **2**, 57–70 (2015).
 - [8] Alexander V. Kolobov and Junji Tominaga, *Two-Dimensional Transition-Metal Dichalcogenides* (Springer International Publishing, 2016).
 - [9] Gang Wang, Alexey Chernikov, Mikhail M. Glazov, Tony F. Heinz, Xavier Marie, Thierry Amand, and Bernhard Urbaszek, “Colloquium: Excitons in atomically thin transition metal dichalcogenides,” *Rev. Mod. Phys.* **90**, 021001 (2018).
 - [10] M V Durnev and M M Glazov, “Excitons and trions in two-dimensional semiconductors based on transition metal dichalcogenides,” *Physics-Uspekhi* **61**, 825–845 (2018).
 - [11] Zhipeng Li, Tianmeng Wang, Shengnan Miao, Zhen Lian, and Su-Fei Shi, “Fine structures of valley-polarized excitonic states in monolayer transitional metal dichalcogenides,” *Nanophotonics* **9**, 1811–1829 (2020).
 - [12] Archana Raja, Andrey Chaves, Jaeun Yu, Ghidewon Arefe, Heather M. Hill, Albert F. Rigosi, Timothy C. Berkelbach, Philipp Nagler, Christian Schüller, Tobias Korn, Colin Nuckolls, James Hone, Louis E. Brus, Tony F. Heinz, David R. Reichman, and Alexey Chernikov, “Coulomb engineering of the bandgap and excitons in two-dimensional materials,” *Nature Communications* **8**, 15251 (2017).
 - [13] Archana Raja, Lutz Waldecker, Jonas Zipfel, Yeongsu Cho, Samuel Brem, Jonas D. Ziegler, Marvin Kulig, Takashi Taniguchi, Kenji Watanabe, Ermin Malic, Tony F. Heinz, Timothy C. Berkelbach, and Alexey Chernikov, “Dielectric disorder in two-dimensional materials,” *Nature Nanotechnology* **14**, 832 (2019).
 - [14] C. Robert, M. A. Semina, F. Cadiz, M. Manca, E. Courtade, T. Taniguchi, K. Watanabe, H. Cai, S. Tongay, B. Lassagne, P. Renucci, T. Amand, X. Marie, M. M. Glazov, and B. Urbaszek, “Optical spectroscopy of excited exciton states in MoS₂ monolayers in van der Waals heterostructures,” *Phys. Rev. Materials* **2**, 011001 (2018).
 - [15] H. H. Fang, B. Han, C. Robert, M. A. Semina, D. Lagarde, E. Courtade, T. Taniguchi, K. Watanabe, T. Amand, B. Urbaszek, M. M. Glazov, and X. Marie, “Control of the exciton radiative lifetime in van der Waals heterostructures,” *Phys. Rev. Lett.* **123**, 067401 (2019).
 - [16] You Zhou, Giovanni Scuri, Jiho Sung, Ryan J. Gelly, Dominik S. Wild, Kristiaan De Greve, Andrew Y. Joe, Takashi Taniguchi, Kenji Watanabe, Philip Kim, Mikhail D. Lukin, and Hongkun Park, “Controlling excitons in an atomically thin membrane with a mirror,” *Phys. Rev. Lett.* **124**, 027401 (2020).
 - [17] Christopher Rogers, Dodd Gray, Nathan Bogdanowicz, Takashi Taniguchi, Kenji Watanabe, and Hideo Mabuchi, “Coherent feedback control of two-dimensional excitons,” *Phys. Rev. Research* **2**, 012029 (2020).
 - [18] J. Horng, Y.-H. Chou, T.-C. Chang, C.-Y. Hsu, T.-C. Lu, and H. Deng, “Engineering radiative coupling of excitons in 2d semiconductors,” *Optica* **6**, 1443 (2019).
 - [19] Denis G. Baranov, Alex Krasnok, Timur Shegai, Andrea Alù, and Yidong Chong, “Coherent perfect absorbers: linear control of light with light,” *Nature Reviews Mate-*

- rials **2**, 17064 (2017).
- [20] Giovanni Scuri, You Zhou, Alexander A. High, Dominik S. Wild, Chi Shu, Kristiaan De Greve, Luis A. Jauregui, Takashi Taniguchi, Kenji Watanabe, Philip Kim, Mikhail D. Lukin, and Hongkun Park, “Large excitonic reflectivity of monolayer MoSe₂ encapsulated in hexagonal boron nitride,” *Phys. Rev. Lett.* **120**, 037402 (2018).
 - [21] Patrick Back, Sina Zeytinoglu, Aroosa Ijaz, Martin Kroner, and Atac Imamoglu, “Realization of an electrically tunable narrow-bandwidth atomically thin mirror using monolayer MoSe₂,” *Phys. Rev. Lett.* **120**, 037401 (2018).
 - [22] K. L. Koshelev, S. K. Sychev, Z. F. Sadrieva, A. A. Bogdanov, and I. V. Iorsh, “Strong coupling between excitons in transition metal dichalcogenides and optical bound states in the continuum,” *Phys. Rev. B* **98**, 161113 (2018).
 - [23] Alex Krasnok, Sergey Lepeshov, and Andrea Alú, “Nanophotonics with 2d transition metal dichalcogenides,” *Opt. Express* **26**, 15972–15994 (2018).
 - [24] Xiaodong Xu, Wang Yao, Di Xiao, and Tony F. Heinz, “Spin and pseudospins in layered transition metal dichalcogenides,” *Nat Phys* **10**, 343–350 (2014).
 - [25] Di Xiao, Gui-Bin Liu, Wanxiang Feng, Xiaodong Xu, and Wang Yao, “Coupled spin and valley physics in monolayers of MoS₂ and other group-VI dichalcogenides,” *Phys. Rev. Lett.* **108**, 196802 (2012).
 - [26] Kin Fai Mak, Keliang He, Jie Shan, and Tony F. Heinz, “Control of valley polarization in monolayer MoS₂ by optical helicity,” *Nat Nano* **7**, 494–498 (2012).
 - [27] G. Sallen, L. Bouet, X. Marie, G. Wang, C. R. Zhu, W. P. Han, Y. Lu, P. H. Tan, T. Amand, B. L. Liu, and B. Urbaszek, “Robust optical emission polarization in MoS₂ monolayers through selective valley excitation,” *Phys. Rev. B* **86**, 081301 (2012).
 - [28] G. Kiioseoglou, A. T. Hanbicki, M. Currie, A. L. Friedman, D. Gunlycke, and B. T. Jonker, “Valley polarization and intervalley scattering in monolayer MoS₂,” *Applied Physics Letters* **101**, 221907 (2012).
 - [29] Hualing Zeng, Junfeng Dai, Wang Yao, Di Xiao, and Xiaodong Cui, “Valley polarization in MoS₂ monolayers by optical pumping,” *Nat Nano* **7**, 490–493 (2012).
 - [30] Aaron M. Jones, Hongyi Yu, Nirmal J. Ghimire, Sanfeng Wu, Grant Aivazian, Jason S. Ross, Bo Zhao, Jiaqiang Yan, David G. Mandrus, Di Xiao, Wang Yao, and Xiaodong Xu, “Optical generation of excitonic valley coherence in monolayer WSe₂,” *Nat Nano* **8**, 634–638 (2013).
 - [31] Hongyi Yu, Gui-Bin Liu, Pu Gong, Xiaodong Xu, and Wang Yao, “Dirac cones and Dirac saddle points of bright excitons in monolayer transition metal dichalcogenides,” *Nat Commun* **5**, 3876 (2014).
 - [32] Malte Selig, Florian Katsch, Robert Schmidt, Steffen Michaelis de Vasconcellos, Rudolf Bratschitsch, Ermin Malic, and Andreas Knorr, “Ultrafast dynamics in monolayer transition metal dichalcogenides: Interplay of dark excitons, phonons, and intervalley exchange,” *Phys. Rev. Research* **1**, 022007 (2019).
 - [33] Keisuke Shinokita, Xiaofan Wang, Yuhei Miyauchi, Kenji Watanabe, Takashi Taniguchi, and Kazunari Matsuda, “Continuous control and enhancement of excitonic valley polarization in monolayer WSe₂ by electrostatic doping,” *Advanced Functional Materials* **29**, 1900260 (2019).
 - [34] Yanhao Tang, Kin Fai Mak, and Jie Shan, “Long valley lifetime of dark excitons in single-layer WSe₂,” *Nature Communications* **10**, 4047 (2019).
 - [35] S. Dufferwiel, T. P. Lyons, D. D. Solnyshkov, A. A. P. Trichet, F. Withers, S. Schwarz, G. Malpuech, J. M. Smith, K. S. Novoselov, M. S. Skolnick, D. N. Krizhanovskii, and A. I. Tartakovskii, “Valley-addressable polaritons in atomically thin semiconductors,” *Nature Photonics* **11**, 497 (2017).
 - [36] Min Yang, Cedric Robert, Zhengguang Lu, Dinh Van Tuan, Dmitry Smirnov, Xavier Marie, and Hanan Dery, “Exciton valley depolarization in monolayer transition-metal dichalcogenides,” *Phys. Rev. B* **101**, 115307 (2020).
 - [37] M. Selig, F. Katsch, S. Brem, G. F. Mkrtchian, E. Malic, and A. Knorr, “Suppression of intervalley exchange coupling in the presence of momentum-dark states in transition metal dichalcogenides,” *Phys. Rev. Research* **2**, 023322 (2020).
 - [38] M. M. Glazov, T. Amand, X. Marie, D. Lagarde, L. Bouet, and B. Urbaszek, “Exciton fine structure and spin decoherence in monolayers of transition metal dichalcogenides,” *Phys. Rev. B* **89**, 201302 (2014).
 - [39] M. M. Glazov, E. L. Ivchenko, G. Wang, T. Amand, X. Marie, B. Urbaszek, and B. L. Liu, “Spin and valley dynamics of excitons in transition metal dichalcogenide monolayers,” *physica status solidi (b)* **252**, 2349–2362 (2015).
 - [40] T. Yu and M. W. Wu, “Valley depolarization dynamics and valley Hall effect of excitons in monolayer and bilayer MoS₂,” *Phys. Rev. B* **93**, 045414 (2016).
 - [41] M.Z. Maialle, E.A. de Andrada e Silva, and L.J. Sham, “Exciton spin dynamics in quantum wells,” *Phys. Rev. B* **47**, 15776 (1993).
 - [42] S. V. Goupalov, E. L. Ivchenko, and A. V. Kavokin, “Fine structure of localized exciton levels in quantum wells,” *JETP* **86**, 388 (1998).
 - [43] E. L. Ivchenko, *Optical spectroscopy of semiconductor nanostructures* (Alpha Science, Harrow UK, 2005).
 - [44] G. E. Pikus and G. L. Bir, “Exchange interaction in excitons in semiconductors,” *JETP* **33**, 108 (1971).
 - [45] M. M. Denisov and V. P. Makarov, “Longitudinal and transverse excitons in semiconductors,” *Physica Status Solidi (b)* **56**, 9–59 (1973).
 - [46] G. L. Bir and G. E. Pikus, *Symmetry and Strain-induced Effects in Semiconductors* (Wiley/Halsted Press, 1974).
 - [47] F. Cadiz, E. Courtade, C. Robert, G. Wang, Y. Shen, H. Cai, T. Taniguchi, K. Watanabe, H. Carrere, D. Lagarde, M. Manca, T. Amand, P. Renucci, S. Tongay, X. Marie, and B. Urbaszek, “Excitonic linewidth approaching the homogeneous limit in MoS₂-based van der Waals heterostructures,” *Phys. Rev. X* **7**, 021026 (2017).
 - [48] O. A. Ajayi, J. V. Ardelean, G. D. Shepard, J. Wang, A. Antony, T. Taniguchi, K. Watanabe, T. F. Heinz, S. Strauf, X.-Y. Zhu, and J. C. Hone, “Approaching the intrinsic photoluminescence linewidth in transition metal dichalcogenide monolayers,” *2D Materials* **4**, 031011 (2017).
 - [49] Yeongsu Cho and Timothy C. Berkelbach, “Environmentally sensitive theory of electronic and optical transitions in atomically thin semiconductors,” *Phys. Rev. B* **97**, 041409 (2018).
 - [50] I. C. Gerber and X. Marie, “Dependence of band structure and exciton properties of encapsulated WSe₂ monolayers on the hBN-layer thickness,” *Phys. Rev. B* **98**, 245126 (2018).

- [51] V. A. Kiselev and A. G. Zhilich, “On dielectric theory of semiconductors with account for excitons,” *Sov. Phys. - Semicond.* **8**, 411 (1974).
- [52] V. A. Kiselev and A. G. Zhilich, “Effective screening of the short-range exchange interaction in excitons,” *Phys. Solid. State* **15**, 1351 (1974).
- [53] L.D. Landau and E.M. Lifshitz, *Electrodynamics of Continuous Media (vol. 8)* (Butterworth-Heinemann, Oxford, 2004).
- [54] M.I. Dyakonov and V.I. Perel’, “Spin relaxation of conduction electrons in noncentrosymmetric semiconductors,” *Sov. Phys. Solid State* **13**, 3023 (1972).
- [55] Malte Selig, Gunnar Berghäuser, Marten Richter, Rudolf Bratschitsch, Andreas Knorr, and Ermin Malic, “Dark and bright exciton formation, thermalization, and photoluminescence in monolayer transition metal dichalcogenides,” *2D Materials* **5**, 035017 (2018).
- [56] Ioannis Paradisanos, Gang Wang, Evgeny M. Alexeev, Alisson R. Cadore, Xavier Marie, Andrea C. Ferrari, Mikhail M. Glazov, and Bernhard Urbaszek, “Efficient phonon cascades in hot photoluminescence of WSe₂ monolayers,” [arXiv:2007.05369](https://arxiv.org/abs/2007.05369) (2020).
- [57] M. M. Glazov, “Quantum interference effect on exciton transport in monolayer semiconductors,” *Phys. Rev. Lett.* **124**, 166802 (2020).
- [58] M. M. Glazov, “Effect of structure anisotropy on low temperature spin dynamics in quantum wells,” *Solid State Commun.* **142**, 531 (2007).
- [59] H. Nickolaus, H.-J. Wünsche, and F. Henneberger, “Exciton spin relaxation in semiconductor quantum wells: The role of disorder,” *Phys. Rev. Lett.* **81**, 2586–2589 (1998).
- [60] V. N. Gridnev, “Theory of Faraday rotation beats in quantum wells with large spin splitting,” *JETP Letters* **74**, 380 (2001).
- [61] C. R. Zhu, K. Zhang, M. Glazov, B. Urbaszek, T. Amand, Z. W. Ji, B. L. Liu, and X. Marie, “Exciton valley dynamics probed by Kerr rotation in WSe₂ monolayers,” *Phys. Rev. B* **90**, 161302 (2014).
- [62] M. A. Brand, A. Malinowski, O. Z. Karimov, P. A. Marsden, R. T. Harley, A. J. Shields, D. Sanvitto, D. A. Ritchie, and M. Y. Simmons, “Precession and motional slowing of spin evolution in a high mobility two-dimensional electron gas,” *Phys. Rev. Lett.* **89**, 236601 (2002).